ACS Photonics

Article

pubs.acs.org/journal/apchd5

Metal Nanogrid for Broadband Multiresonant Light-Harvesting in Ultrathin GaAs Layers

Inès Massiot,[†] Nicolas Vandamme,[†] Nathalie Bardou,[†] Christophe Dupuis,[†] Aristide Lemaître,[†] Jean-François Guillemoles,[‡] and Stéphane Collin*[,†]

[†]Laboratoire de Photonique et de Nanostructures (LPN-CNRS), Route de Nozay, 91460 Marcoussis, France

[‡]Institut de Recherche et Développement sur l'Energie Photovoltaïque (IRDEP-UMR 7174 CNRS/EDF/Chimie-ParisTech), 6 quai Watier, 78401 Chatou, France

ABSTRACT: Most plasmonic super absorbers use the excitation of surface plasmons to achieve perfect absorption in metal nanostructures. We present a design for an ultrathin metal−semiconductor−metal super absorber where light is mainly absorbed within a flat 25 nm thick GaAs semiconductor layer. The top metal layer is patterned as a two-dimensional grid with a subwavelength period and is covered with a thin embedding dielectric layer. We show numerically multiresonant absorption with low polarization and angular dependence. We experimentally demonstrate optical absorption above 80% over the 450−830 nm spectral range using a gold nanogrid. This work opens perspectives toward ultrathin active plasmonic optoelectronic devices and, in particular, highly efficient ultrathin solar cells.

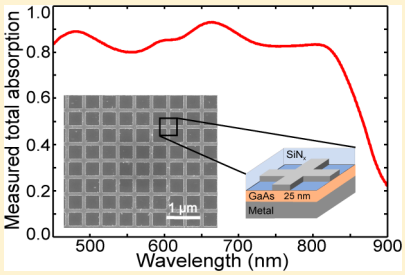

KEYWORDS: *plasmonics, super absorbers, broadband absorption, ultrathin, solar cell*

The ability of plasmonic structures to confine and control light at the nanoscale has opened new perspectives for ultrathin optoelectronic devices. For instance, reducing the absorber thickness is the main importance for several photovoltaic technologies because of the material cost, its scarcity, or its stability issues. In this article, we address the issue of the reduction of the absorber volume by more than 1 order of magnitude while keeping high absorption efficiency on a broad spectral range. Photocurrent enhancement has already been experimentally demonstrated in ultrathin (thickness = 100−200 nm) amorphous silicon solar cells with silver gratings integrated in the back contact of the cell.[1−3] The absorption enhancement was attributed to the excitation of guided modes via coupling to the metal grating. It is however restricted to a limited spectral domain close to the bandgap. Absorption enhancement in very small semiconductor volumes in GaAs-based metal−semiconductor−metal (MSM) photodetectors has also been demonstrated but in a very narrow spectral range.[4,5] Furthermore, growing the active layer on a patterned substrate creates defective areas that induce shunt currents in the solar cells.[6] The development of novel solutions of light trapping over a much broader spectral range, and within planar semiconducting layers, is a major challenge.

On the other hand, perfect absorption has been achieved in various plasmonic nanocavities. Using surface plasmon polaritons (SPP) localized in metal nanostructures, incident light can be totally absorbed in the metal on a spectral range that can be tuned in the visible,[7−10] infrared,[10−12] or terahertz regime,[13] depending on the geometrical parameters of the nanostructures. However, for many applications to photon-absorbing devices, ideal plasmonic absorbers should exhibit perfect absorption on a broad range of wavelengths and incident angles. One approach developed relies on subwavelength-period arrays of ultrasharp convex grooves to achieve plasmonic black gold[9,10] or nickel.[10] Søndergaard et al. have already shown that an average absorption level of 96% of unpolarized light over a broad spectral range (450−850 nm) could be achieved with this approach.[9] Another strategy relies on metal−insulator−metal (MIM) structures with a patterned top metal layer.[7,8,12,13] The absorption spectral range depends on the geometry and size of the nanopatterns and is limited in most cases to a single resonant mode. Aydin et al. have proposed to use the width variation along a trapezoid to broaden the absorption spectrum compared to stripe arrays.[7] They have demonstrated experimentally an average total absorption of 71% on the 400−700 nm wavelength range using a crossed trapezoidal array as the top-structured metal layer. Nevertheless, in order to design active optoelectronic devices, such as solar cells, the absorption should be routed in active semiconductor materials instead of metals. The existing approaches are thus limited to thermal applications where light is fully absorbed in the metal.

Previous numerical works have proposed MSM designs for broadband light-trapping in ultrathin amorphous silicon solar cells using one-dimensional silver wires[14,15] or a nanopatterned checkerboard silver film.[16] In this article, we demonstrate experimentally broadband absorption in an MSM structure based on a flat and ultrathin (25 nm) GaAs layer. The combination of a 2D subwavelength metal nanogrid and an embedding dielectric material leads to a broadband and omnidirectional multiresonant absorption spectrum. We report

Received: May 17, 2014
Published: August 26, 2014

experimental super absorbers based on ultrathin GaAs layers with a polarization-independent absorption over 80% between 450 and 830 nm. The semitransparency and high conductivity of the metal nanogrid also enable its use as an alternative electrode replacing standard conductive oxides for applications as flexible optoelectronic devices for instance. This ultrathin super absorber structure thus opens new perspectives for high-efficient plasmonic solar cells.

DESIGN OF ULTRATHIN GAAS-BASED SUPER ABSORBERS

Our broadband absorber design consists of a MSM structure with the top metal layer nanopatterned as a 2D metal grid, as illustrated in Figure 1. The grid is embedded in a top dielectric layer made of 80 nm of silicon nitride (SiN_x). In this article, we consider a proof-of-concept structure based on an ultrathin 25 nm thick nonintentionally doped GaAs layer as the semiconductor film.

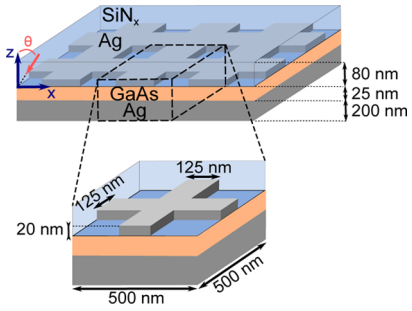

Figure 1. (Top) Schematic of an ultrathin MSM structure with a two-dimensional metal nanogrid. (Bottom) Schematic of the unit cell made of two crossed gratings: length = 500 nm, width = 125 nm, thickness = 20 nm.

Fully vectorial electromagnetic rigorous coupled wave analysis (RCWA) calculations of the MSM structure were performed using the *Reticolo* software developed by P. Lalanne and co-workers.[17−19] The absorption in each layer of the structure is determined from the exact resolution of Maxwell equations using a Fourier decomposition. The unit cell used for the calculations is made of two crossed metal wires with equal widths (125 nm), lengths (500 nm), and thicknesses (20 nm), as shown in Figure 1. The grid is thus periodic along both the x and y axes, with a periodicity of 500 nm. In this section, the metal constituting both the grid and the back mirror is silver. Optical constants are taken from ref 20 for GaAs and the silicon nitride material (Si_3N_4) and from ref 21 for Ag. In order to ensure the convergence of the computation, the calculations are done with M_x and M_y Fourier harmonics along the x and y directions, respectively. In the case of this article, we have found that, for $M_x = M_y \geq 20$, the relative variations in position and amplitude of the absorption peaks are lower than 2 and 0.8%, respectively. In the following, unless otherwise specified, all calculations have been done for $M_x = M_y = 20$.

Figure 2a displays the multiresonant absorption spectrum resulting from numerical optimizations. The structure parameters are chosen to obtain several resonances regularly spaced along the visible spectral range. We show that the coupling of the metal grid to the ultrathin GaAs layer and the metal mirror leads to a multiresonant absorption spectrum with five main absorption peaks at λ = 517, 606, 650−710, 802, and 881 nm. As it can be seen in Figure 2a, the optical response of the MSM structure presented in this article exhibits two remarkable properties that are discussed in the following: (i) a high absorption efficiency within the semiconductor layer and (ii) a broad absorption band with a low polarization and angular dependence.

It is noteworthy that the total absorption is higher than 0.9 at each resonance wavelength. In particular, for the long wavelength resonances (802 and 881 nm), perfect absorption is achieved in the structure: the critical coupling condition is fulfilled for these two resonances.[22] Furthermore, the absorption fraction in the semiconductor layer is kept high over the entire spectral range. In order to assess parasitic losses in the metal, we have calculated the mean value of the absorption fraction in the metal (grid + mirror) between λ = 350 and 900 nm and normalized it with respect to the total absorption averaged over the same spectral range. At normal incidence, only 14.9% of absorbed photons are lost in the metal, which means that more than 85% of absorbed photons are absorbed in the very thin semiconductor layer (on average over the 350−900 nm range).

In order to provide a better understanding of the absorption mechanism at stake, we have studied the spatial distribution of the electric field intensity at the five main resonance wavelengths (λ = 517, 606, 711, 802, and 881 nm), as displayed in Figure 2b−f. The structure is excited at normal incidence with a transverse magnetic field, hence, an in-plane electric field. According to the study of the influence of the layer thicknesses (not shown here), the absorption peaks at short wavelengths (517 and 606 nm) can be attributed to vertical Fabry−Perot resonances in the GaAs layer. The spectral splitting of this resonant mode is due to the existence of two

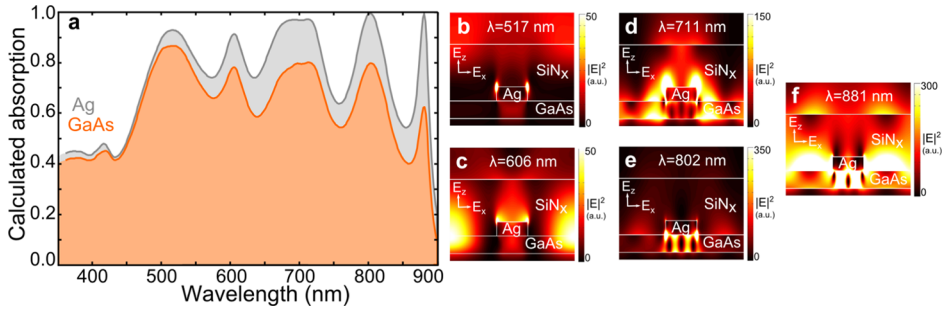

Figure 2. (a) Calculated absorption fraction in the GaAs layer (orange) and silver (top grid + back mirror; gray) at normal incidence. (b−f) Maps of the electric field intensity $|E^2|$ at λ = 517, 606, 711, 802, and 881 nm for an excitation at normal incidence. All the intensity maps have the same unit. The calculations have been done for $M_x = M_y = 30$.

dx.doi.org/10.1021/ph500168b | ACS Photonics 2014, 1, 878−884

resonators with the Fabry–Perot cavity located either below the metal wires (Ag/GaAs/Ag) or the grid holes (SiN_x/GaAs/Ag). The resonance wavelength increases for higher values of the real part of the top material index. The peak attributed to Ag/GaAs/Ag resonances (at 517 nm, Figure 2b) is thus blueshifted with respect to SiN_x/GaAs/Ag resonances (at 606 nm, Figure 2c). At long wavelengths (802 and 881 nm), the electric field intensity $|E^2|$ maps suggest that the absorption enhancement is due to the coupling of surface plasmons propagating on the top (Ag/GaAs) and bottom (GaAs/Ag) interfaces. The Ag/GaAs/Ag cavities play the role of horizontal Fabry–Perot resonators.[22,23] The resonance wavelength of this third-order localized plasmonic mode depends strongly on the resonator size, that is, the width of the metal wires. Surface plasmons are also excited on the GaAs/Ag bottom interface through the holes of the nanogrid. The strong field enhancement in the vicinity of the metal leads to increased parasitic losses at long wavelengths, as can be seen in Figure 2a. Regarding the resonance at 711 nm, the spatial distribution of the electric field intensity (Figure 2d) is more complex. It exhibits maxima under the grid holes characteristic from vertical resonances in the GaAs layer as well as a maximum under the metal wires similar to localized plasmonic modes.

It is worth noticing that the parasitic absorption in the back mirror can be reduced by adding a low index spacing layer below the GaAs layer to shift the field maxima from the GaAs/Ag interface into the semiconductor layer. The index and thickness of the spacing layer would then provide additional degrees of freedom to tune both the intensity and position of the absorption peaks, as discussed in ref 15.

As displayed in Figure 2a, the combination of multiple resonances leads to a broad absorption band. In order to assess the broadband character of the absorption in the structure and its potential for photovoltaics applications, we define the theoretical short-circuit current density as follows:

$$J_{th}(\theta) = \frac{q}{\hbar c}\int A(\lambda, \theta)P(\lambda)\lambda d\lambda \quad (1)$$

where q is the electron charge, $\hbar$ is Planck's constant, c is the speed of light, and θ is the angle of incidence. J_{th} corresponds to the absorption fraction in the semiconductor $A(\lambda)$ integrated for wavelengths greater than 350 nm and weighted by the incident spectral power density per unit area $P(\lambda)$. J_{th} is thus expressed in mA/cm^2. A high value of J_{th} reflects high absorption intensity values as well as a wide absorption band in accordance with the source spectrum. We have considered the solar spectrum as the excitation source, $P(\lambda)$ is then the power density associated with the normalized AM1.5G solar spectrum. The calculation of J_{th} with eq 1 assumes a perfect collection of generated carriers in the device.

We predict a value of J_{th} equal to 21.6 mA/cm^2 at normal incidence for the structure with a 25 nm thick GaAs layer depicted in Figure 1. We have defined a reference structure made of a GaAs film on a silver mirror, with an antireflection coating (ARC) composed of MgF_2 (109 nm) and ZnS (63 nm) layers, the thicknesses of these layers being chosen to reach the highest current for a 1 μm thick GaAs layer. As shown in Table 1, the J_{th} value in this case is 30.3 mA/cm^2, similar to the current experimental records for GaAs solar cells. For a 200 nm thick reference structure, the short-circuit current density is equal to 22.2 mA/cm^2, very close to the value we demonstrate numerically for the MSM nanogrid structure with a 25 nm thick GaAs layer. We have thus shown that we can reduce the GaAs thickness almost by a factor eight using the metal nanogrid to trap light within the semiconductor layer. It is also noteworthy that the MSM nanogrid structure exhibits a 2-fold enhancement of the short-circuit current compared to the reference structure with 25 nm of GaAs.

Table 1. Performance of the MSM Nanogrid Structure Compared to Reference Cells of Varying GaAs Thicknesses and Experimental Record GaAs Solar Cells[24,25]

structure	GaAs thickness	short-circuit current density
SiN_x/GaAs/Ag with nanogrid	25 nm	21.6 mA/cm^2
GaAs on Ag with ARC	25 nm	10.9 mA/cm^2
GaAs on Ag with ARC	200 nm	22.2 mA/cm^2
GaAs on Ag with ARC	1 μm	30.3 mA/cm^2
record GaAs cells (exp.)	1–2 μm	29.6,[24] 29.46[25] mA/cm^2

Figure 3a,b displays the evolution of the total absorption in the structure as a function of the excitation wavelength and the angle of incidence θ defined in the plane of incidence (xz), as illustrated in the insets, for transverse electric (TE; Figure 3a) and transverse magnetic (TM; Figure 3b) polarizations. It should be noted that our structure combines both non-dispersive and dispersive modes and therefore should be sensitive to the angle of incidence. Below 850 nm, the spectral

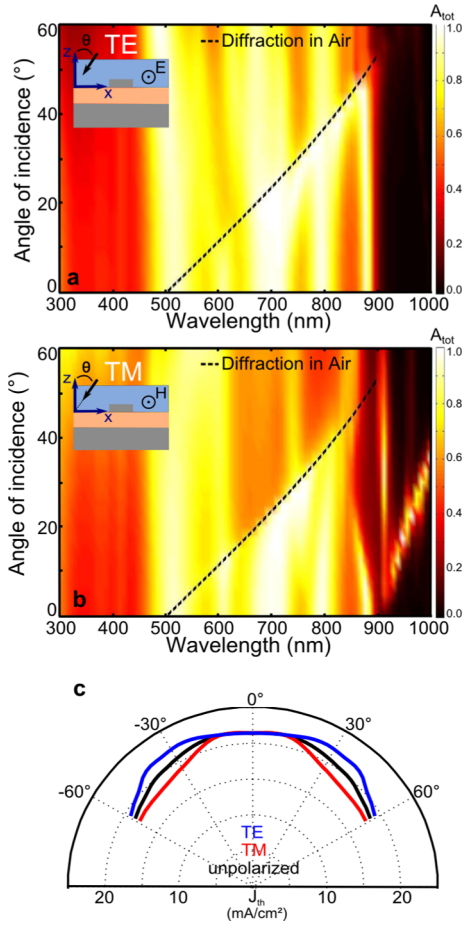

Figure 3. (a,b) Total absorption in the structure as a function of the angle of incidence and the wavelength for TE (a) and TM (b) polarizations. Diffraction orders in air exist above the dashed black curves. (c) Theoretical short-circuit current density J_{th} (eq 1) as a function of the angle of incidence varying from 0° to 60°.

dx.doi.org/10.1021/ph500168b | ACS Photonics 2014, 1, 878–884

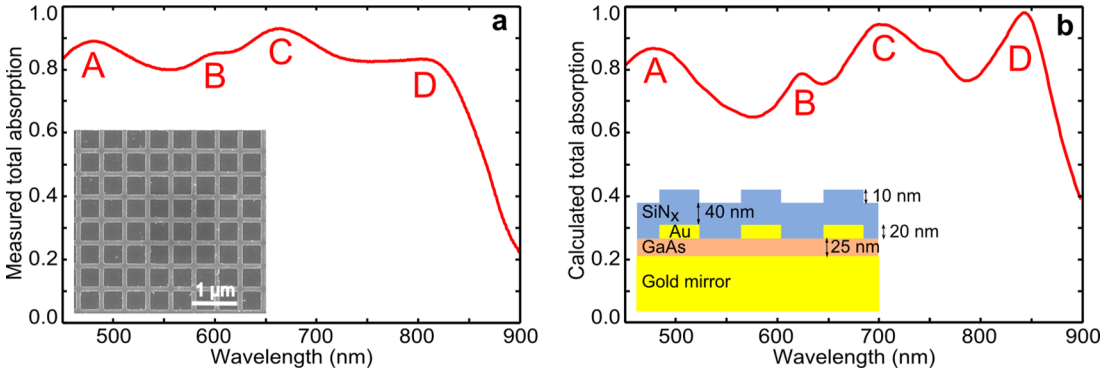

Figure 4. Measured (a) and calculated (b) total absorption spectra at normal incidence of the SiN_x(Au)/GaAs/Au structure. Inset of (a): SEM image of the 2D gold nanogrid. Inset of (b): schematic of the structure modeled with a rectangular surface profile.

position of the absorption peaks is independent from the angle of incidence for both polarizations, which confirms the localized nature of the resonances involved. At longer wavelengths, the resonance spectral location depends on θ and additional peaks appear at non-normal incidence.

In order to quantify the angular dependence of the structure, we have calculated J_{th}, as defined in eq 1 for an angle of incidence θ varying between 0° and 60°. The result is shown in Figure 3c. The current density value J_{th} for unpolarized incident light (black) is calculated as the average of the values for TE (blue) and TM (red) polarizations. For both polarizations, the existence of diffracted orders in free-space induces intensity losses for oblique incidence. The curve above which diffracted orders in air exist is shown in dashed black line for both polarizations. In TM polarization, a significant decrease of J_{th} is thus shown for angles higher than 15°. However, in TE polarization, light incoupling seems to be more efficient for angles between 20° and 40° than at normal incidence. As a consequence, the nanogrid structure shows a weak angular dependence. At 60°, J_{th} is equal to 18.6 mA/cm^2, which represents 86% of the value at normal incidence (21.6 mA/cm^2).

Our numerical study thus shows that MSM nanogrid structures can be used to confine light absorption within a 25 nm thick semiconductor layer. We have also shown that the 2D metal nanogrid structure leads to a multiresonant broadband absorption with a low polarization and angular dependence. Moreover, the 2D design provides another functionality to the grid as it may serve as an alternative front electrode. The subwavelength ultrathin nanogrid is semitransparent: as shown in Figure 2a, absorption in the semiconductor exceeds 70% at resonances, whereas more than 43% of the absorber surface is covered by metal. In order to assess the conductivity of the metal nanogrid, we calculated its sheet resistivity using $R_s = (\rho p/h_m w)$ with $\rho = 1.6.10^{-8}$ Ω·m the bulk resistivity of Ag, p = 500 nm the grid period, w = 125 nm the grid finger width, and h_m = 20 nm the metal thickness.[26] We find R_s = 3.2 Ω/square, which is a better conductivity than conventional conductive oxides, such as ITO.[27] Metal nanogrids offer a low sheet resistance and thus can be used as an alternative front electrode.

FABRICATION OF METAL NANOGRIDS ON ULTRATHIN GAAS/AU LAYERS

The proof-of-concept structure illustrated in Figure 1a has been fabricated by transferring an ultrathin crystalline GaAs layer on a host substrate. For technological reasons, Au was used instead of Ag as the metal constituting both the nanogrid and the back mirror. First, ultrathin crystalline GaAs layers with a nominal thickness of 25 nm were grown by molecular beam epitaxy on a GaAs substrate with a 300 nm thick $Al_{0.8}Ga_{0.2}As$ etch-stop layer. Then, a 200 nm thick Au layer was deposited onto the GaAs layer by electron-beam assisted evaporation after deoxidation of the GaAs surface in a hydrochloric solution. Prior to bonding onto a Pyrex substrate, 200 nm of Al were deposited by electron-beam assisted evaporation with a Ti barrier layer between Au and Al to avoid diffusion during bonding. The anodic bonding of Al to Pyrex was performed with a SUSS MicroTec substrate bonder at 1700 V for 80 min, with a maximum temperature of 210 °C. The initial GaAs substrate was etched in a NH_4OH/H_2O_2 solution and the AlGaAs etch-stop layer was removed in a HF solution with a 10% concentration for a few seconds. The grid nanopatterning was done by electron beam lithography on a PMMA A5 resist. A total of 20 nm of Au were then deposited on the patterned resist by electron beam evaporation with a 1 nm thick Ge nucleation layer. The lift-off of the resist was performed in a hot trichloroethylene solution (80 °C) with soft magnetic stirring. Finally, a 60 nm thick silicon nitride layer was deposited by RF magnetron sputtering onto the Au/GaAs/Au structure. A scanning electron microscope (SEM) image of the fabricated structure is shown in the inset of Figure 4a. The effective thickness of the GaAs layer has been evaluated to 23 nm from reflectivity measurements.

EXPERIMENTAL EVIDENCE OF MULTIRESONANT BROADBAND ABSORPTION

The performances of our device were analyzed through total reflectivity (R) measurements at normal incidence. We assume that there is no transmission through the substrate as the samples are patterned on a 200 nm thick gold back mirror. Its thickness is indeed much greater than the skin depth of the metal in the visible (δ = 25 nm at 500 nm). Light scattering caused by inhomogeneities has also been neglected. Moreover, there is no diffraction in free space for wavelengths greater than the period of the grid at normal incidence. For wavelengths below 500 nm, diffraction affects less than 1% of the incident light according to numerical calculations and is therefore neglected in the following. The total absorption A in the structure can then be deduced from $A = 1 - R$.

Figure 4a displays the measured total absorption at normal incidence for a SiN_x(Au)/GaAs/Au structure with the following nanogrid parameters: period = 500 nm, width = 125 nm, thickness = 20 nm. The total absorption spectrum exhibits four main resonances leading to a multiresonant absorption band on

dx.doi.org/10.1021/ph500168b | ACS Photonics 2014, 1, 878−884

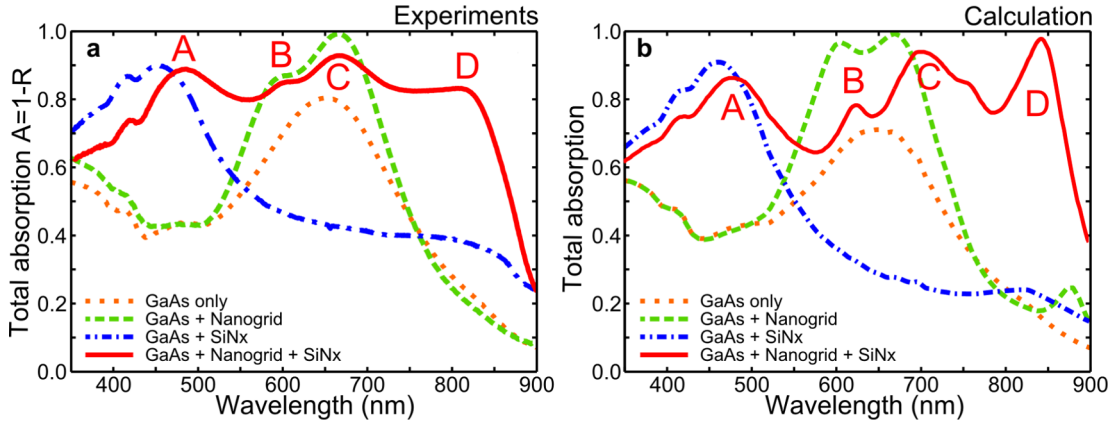

Figure 5. Comparison between (a) experimental absorption measurements and (b) the corresponding calculations for each step of the fabrication process.

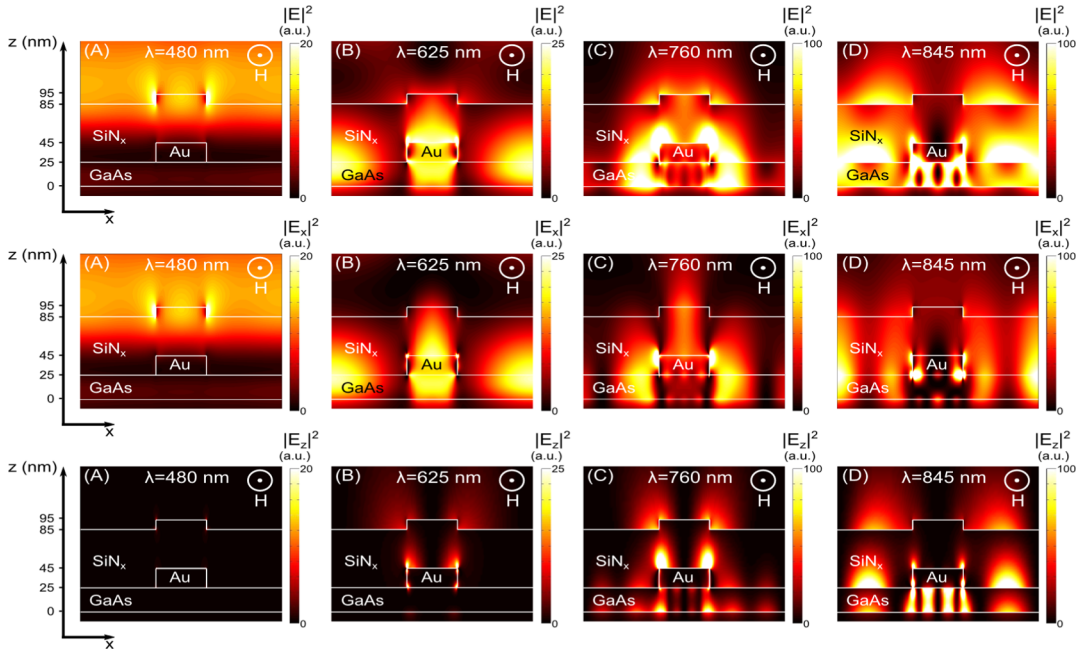

Figure 6. Maps of the intensity of the electric field components ($|E^2|$, $|E_x^2|$ and $|E_z^2|$) for λ = 480, 625, 760, and 845 nm for the Au/GaAs/Au nanogrid structure described in Figure 4b (GaAs thickness = 25 nm, grid thickness = 20 nm, grid period = 500 nm, grid width = 125 nm). The sample is excited at normal incidence with a transverse magnetic field. All the intensity maps have the same unit for each resonance. The calculations have been done for $M_x = M_y = 30$.

a very large wavelength range. For $\lambda > 850$ nm, the absorption intensity drops in accordance with the increased absorption depth of bulk GaAs (bandgap E_g = 1.42 eV).

It is noteworthy that we have demonstrated experimentally an absorption intensity over 80% between 450 and 830 nm. We have thus shown a broader absorption band than reported by Aydin et al.[7] (average total absorption at normal incidence of 71% between 400 and 700 nm) with an absorption level very close to Søndergaard et al.[9] (total absorption over 87% on 450−850 nm). Furthermore, in the aforementioned approaches, light is absorbed entirely in the metal, whereas most of the absorption is expected to occur in the semiconductor in our case, as predicted by RCWA calculations. Such a property is absolutely necessary in order to integrate efficiently plasmonic structures into active optoelectronic devices. To our knowledge, we report the broadest absorption band demonstrated experimentally for such an ultrathin semiconductor layer (23 nm).

We have performed electromagnetic simulations to evaluate numerically the absorption in the fabricated SiN_x(Au)/GaAs/Au structure. These calculations take into account the nominal thickness of the transferred GaAs layer (25 nm), and the surface profile of the silicon nitride coating. The result of the calculation is displayed in Figure 4b: the inset illustrates the rectangular surface profile that we have considered in order to account for the conformal deposition of silicon nitride on the patterned metal film. The calculated spectrum is in good accordance with the measurements. Especially, both spectra feature the four resonance peaks A−D. It should be noted that the resonances are broader on the experimental absorption spectrum, which can be attributed to the width variation along the fabricated grid. The resonance wavelengths are in good agreement, except for the C resonance, which is blueshifted by

dx.doi.org/10.1021/ph500168b | ACS Photonics 2014, 1, 878−884

approximately 50 nm in the experiments. The simulations displayed in Figure 4b also allow us to estimate that 51% of absorbed photons in the fabricated structure are absorbed within the 25 nm thick semiconductor layer, on average over the 350−900 nm spectral range. The other 49% are lost either in the metal grid or the back mirror. The absorption losses in the metal are expected to be reduced significantly by replacing the gold used both for the nanogrid and the mirror by silver as in the design presented previously.

We can isolate the influence of the different elements of the MSM nanogrid structure on total absorption by measuring the reflectivity of the sample after each technological step. Figure 5 shows the measured absorption spectra ($A = 1 - R$) and the corresponding numerical calculations along the fabrication process. Remarkable accordance has been evidenced between calculations and experimental measurements. The total absorption for the GaAs layer transferred on gold (orange dotted lines) consists of a single Fabry−Perot resonance around 650 nm. When the nanogrid is deposited, this Fabry−Perot mode is splitted in the two resonances B and C at 580 and 670 nm, respectively (green dashed lines). Finally, the comparison between the nanogrid structure with/without top coating (red/green curves, respectively) shows that the silicon nitride layer plays a major role in the apparition of resonances A and D, greatly widening the absorption spectrum. At short wavelengths, it supplies an antireflection effect to the structure, as can be shown on the response of the structure GaAs + coating shown in blue dashed-dotted lines (no nanogrid). In addition, the absorption intensity at 850 nm is greatly enhanced from 15 to 83% with silicon nitride (see Figure 5). Deposition technique and thickness of the silicon nitride layer are key parameters to manage a high level of absorption over the visible spectrum. We noticed, for example, that for 100 nm of silicon nitride (instead of 60 nm), the absorption spectrum was tuned toward longer wavelengths and resonance peaks were narrower, potentially reducing the efficiency of the light-trapping scheme.

To gain insight on the different light-trapping mechanisms, we have plotted the electric field maps at each resonance wavelength in Figure 6. At 480 nm, the field is localized inside the semiconductor layer between $z = 0$ and 25 nm, with a low spatial modulation along the x-axis. Resonance A thus corresponds to a vertical Fabry−Perot in the GaAs layer. As shown in Figure 5, the silicon nitride layer induces a blue shift from 650 nm (GaAs/Au) to 450 nm (SiN_x(Au)/GaAs/Au), but the nanogrid plays a minor role at this wavelength (red shift to 500 nm, resonance A). As expected for a vertical resonance (along z), $|E^2|$ is dominated by the (transverse) $|E_x^2|$ component. This is also the case for resonance B, where the electric field intensity outside the nanostructure spreads on both semiconductor layer and silicon nitride coating between $z = 0$ and $z = 85$ nm. This resonance is also attributed to a vertical Fabry−Perot in the cavity formed by these two layers. Along the z-axis, the electric field maximum is located at $z \simeq 10$ nm for resonance A, and $z \simeq 25$ nm for resonance B. As for peaks C and D, it is noteworthy that field maps present an intensity maximum which is 5−10× higher than for previous resonances. It enables to compensate for the lower absorptivity of GaAs at longer wavelengths. In the case of resonance C, the light-trapping mechanism is more difficult to understand as the field distribution is complex, with variations along both the x- and z-axes, and a similar weight for the $|E_x^2|$ and $|E_z^2|$ component. It may be attributed to a superposition of dispersive and nondispersive modes.

Finally, resonance D at 845 nm exhibits a third-order localized plasmonic resonance under the Au nanostructure. Coupling between SPPs at the two metal/semiconductor interfaces leads to an horizontal oscillation of the electric field. Very high enhancement factors (>100) are reached at field maxima. To quantify light confinement within the cavity, we define an effective index as the ratio between the incident wavelength and its effective value in the cavity: $n_{eff} = \lambda/\lambda_{eff}$. The effective wavelength λ_{eff} is given by $\lambda_{eff} = 2d/m$, where d is the length of the cavity and m the order of the resonance. It represents the distance light must travel to oscillate in phase. The length of the cavity being $d = 125$ nm, the effective wavelength is equal to 83 nm here. The effective index of the mode oscillating in the GaAs under the metal nanogrid is thus greater than 10 for resonance D, that is, approximately 3× the refractive index of bulk GaAs for this wavelength.

CONCLUSION

We have presented the design of an ultrathin super absorber in the visible range based on a MSM structure with a top metal nanogrid. We have shown numerically that in the case of a structure with Ag, more than 85% of the absorbed light (on average 350−900 nm) is confined within the ultrathin semiconductor layer thanks to the metal nanogrid. This high absorption efficiency exhibits a low dependence with respect to both the polarization and the angle of incidence. Proof-of-concept structures were fabricated by patterning a gold nanogrid onto a 23 nm thick crystalline GaAs layer transferred on a gold mirror. Experimental data show that a multiresonant absorption spectrum is achieved with a total absorption efficiency higher than 80% between 450 and 830 nm at normal incidence. To our knowledge, this is the broadest absorption spectrum reported for such a thin (23 nm) crystalline semiconductor material. The analysis of absorption measurements performed at several steps of the fabrication process allow to identify the different absorption mechanisms at stake. We show that this ultrathin MSM nanogrid structure combines Fabry−Perot nanoresonators and localized plasmonic resonances. Being able to confine light absorption in such a thin semiconductor material opens new perspectives for high-efficient plasmonic optoelectronic devices, such as solar cells as well as photodetectors with reduced dark current.

For photovoltaics applications, the conception of ultrathin GaAs solar cells requires additional layers: highly doped layers to create an ultrathin $p-n$ junction, passivation layers, and barriers for the minority carriers in order to maximize the collection efficiency of photogenerated charges. The integration of these layers in slightly thicker structures is likely to modify the spectral position and efficiency of the resonant modes. For instance, increasing the thickness of the GaAs layer will modify the coupling between the SPPs on the Ag/GaAs and GaAs/Ag interfaces and thus the spectral position and intensity of the plasmonic resonances. However, the absorption mechanism in thicker layers may rely on additional resonant modes, as guided modes supported by the semiconductor layer,[15] for instance. Integrating the proposed MSM structures into solar cells also requires to minimize parasitic absorption in the metal. As shown in the article, replacing gold by silver allows to reduce parasitic absorption by a factor three. A low index spacing layer could also be inserted below the GaAs layer to decrease absorption in the back mirror.[15]

In conclusion, metal nanogrids offer an efficient tool to collect both incident photons and photogenerated carriers in

dx.doi.org/10.1021/ph500168b | ACS Photonics 2014, 1, 878−884

ultrathin semiconductor layers. It provides additional degrees of freedom to conceive ultrathin optoelectronic devices, whose conception should take into account more complex stacks of semiconductor layers.

AUTHOR INFORMATION

Corresponding Author

*E-mail: stephane.collin@lpn.cnrs.fr.

Notes

The authors declare no competing financial interest.

ACKNOWLEDGMENTS

The authors gratefully acknowledge C. Colin, P. Lalanne, and C. Sauvan for fruitful discussions and support in numerical calculations. This work was partly supported by the ANR projects 3D-BROM, ULTRACIS-M, and NATHISOL and by the RENATECH network.

REFERENCES

(1) Söderström, K.; Haug, F. J.; Escarré, J.; Cubero, O.; Ballif, C. Photocurrent increase in n-i-p thin film silicon solar cells by guided mode excitation via grating coupler. *Appl. Phys. Lett.* **2010**, *96*, 213508.

(2) Zhu, J.; Hsu, C. M.; Yu, Z.; Fan, S.; Cui, Y. Nanodome solar cells with efficient light management and self-cleaning. *Nano Lett.* **2010**, *10*, 1979−1984.

(3) Ferry, V. E.; Verschuuren, M. A.; Li, H. B. T.; Verhagen, E.; Walters, R. J.; Schropp, R. E. I.; Atwater, H. A.; Polman, A. Light trapping in ultrathin plasmonic solar cells. *Opt. Express* **2010**, *18*, A237−A245.

(4) Collin, S.; Pardo, F.; Teissier, R.; Pelouard, J.-L. Efficient light absorption in metal-semiconductor-metal nanostructures. *Appl. Phys. Lett.* **2004**, *85*, 194−196.

(5) Collin, S.; Pardo, F.; Bardou, N.; Lemaître, A.; Averin, S.; Pelouard, J.-L. Harvesting light at the nanoscale by GaAs-gold nanowire arrays. *Opt. Express* **2011**, *19*, 17293−17297.

(6) Hänni, S.; Alexander, D. T. L.; Ding, L.; Bugnon, G.; Boccard, M.; Battaglia, C.; Cuony, P.; Escarré, J.; Parascandolo, G.; Nicolay, S.; Cantoni, M.; Despeisse, M.; Meillaud, F.; Ballif, C. On the interplay between microstructure and interfaces in high-efficiency microcrystalline silicon solar cells. *IEEE, J. Photovoltaics* **2012**, *2*, 1−6.

(7) Aydin, K.; Ferry, V. E.; Briggs, R. M.; Atwater, H. A. Broadband polarization-independent resonant light absorption using ultrathin plasmonic super absorbers. *Nat. Commun.* **2011**, *2*, 517.

(8) Fang, Z.; Zhen, Y.-R.; Fan, L.; Zhu, X.; Nordlander, P. Tunable wide-angle plasmonic perfect absorber at visible frequencies. *Phys. Rev. B* **2012**, *85*, 245401.

(9) Søndergaard, T.; Novikov, S. M.; Holmgaard, T.; Eriksen, R. L.; Beermann, J.; Han, Z.; Pedersen, K.; Bozhevolnyi, S. I. Plasmonic black gold by adiabatic nanofocusing and absorption of light in ultra-sharp convex grooves. *Nat. Commun.* **2012**, *3*, 969.

(10) Beermann, J.; Eriksen, R. L.; Søndergaard, T.; Holmgaard, T.; Pedersen, K.; Bozhevolnyi, S. I. Plasmonic black metals by broadband light absorption in ultra-sharp convex grooves. *New J. Phys.* **2013**, *15*, 073007.

(11) Teperik, T. V.; Garcia de Abajo, F. J.; Borisov, A. G.; Abdelsalam, M.; Bartlett, P. N.; Sugawara, Y.; Baumberg, J. J. Omnidirectional absorption in nanostructured metal surfaces. *Nat. Photonics* **2008**, *2*, 299−301.

(12) Liu, N.; Mesch, M.; Weiss, T.; Hentschel, M.; Giessen, H. Infrared perfect absorber and its application as plasmonic sensor. *Nano Lett.* **2010**, *10*, 2342−2348.

(13) Diem, M.; Koschny, T.; Soukoulis, C. M. Wide-angle perfect absorber/thermal emitter in the terahertz regime. *Phys. Rev. B* **2009**, *79*, 033101.

(14) Massiot, I.; Colin, C.; Péré-Laperne, N.; Roca i Cabarrocas, P.; Sauvan, C.; Lalanne, P.; Pelouard, J.-L.; Collin, S. Nanopatterned front contact for broadband absorption in ultra-thin amorphous silicon solar cells. *Appl. Phys. Lett.* **2012**, *101*, 163901.

(15) Massiot, I.; Colin, C.; Sauvan, C.; Lalanne, P.; Roca i Cabarrocas, P.; Pelouard, J.-L.; Collin, S. Multi-resonant absorption in ultra-thin silicon solar cells with metallic nanowires. *Opt. Express* **2013**, *21*, A372−A381.

(16) Wang, Y.; Sun, T.; Paudel, T.; Zhang, Y.; Ren, Z.; Kempa, K. Metamaterial-plasmonic absorber structure for high efficiency amorphous silicon solar cells. *Nano Lett.* **2012**, *12*, 440−445.

(17) Moharam, M. G.; Grann, E. B.; Pommet, D. A.; Gaylord, T. K. Formulation for stable and efficient implementation of the rigorous coupled-wave analysis of binary gratings. *J. Opt. Soc. Am. A* **1995**, *12*, 1068−1076.

(18) Lalanne, P.; Morris, G. M. Highly improved convergence of the coupled-wave method for TM polarization. *J. Opt. Soc. Am. A* **1996**, *13*, 779−784.

(19) Lalanne, P.; Jurek, M. P. Computation of the near-field pattern with the coupled-wave method for transverse magnetic polarization. *J. Mod. Opt.* **1998**, *45*, 1357−1374.

(20) Palik, E. *Handbook of Optical Constants of Solids*; Academic Press: Orlando, 1985.

(21) Johnson, P. B.; Christy, R. W. Optical constants of the noble metals. *Phys. Rev. B* **1972**, *6*, 4370−4379.

(22) Cattoni, A.; Ghenuche, P.; Haghiri-Gosnet, A. M.; Decanini, D.; Chen, J.; Pelouard, J. L.; Collin, S. $\lambda^3/1000$ plasmonic nanocavities for biosensing fabricated by soft UV nanoimprint lithography. *Nano Lett.* **2011**, *11*, 3557−3563.

(23) Yang, J.; Sauvan, C.; Jouanin, A.; Collin, S.; Pelouard, J.-L.; Lalanne, P. Ultrasmall metal-insulator-metal nanoresonators: impact of slow-wave effects on the quality factor. *Opt. Express* **2012**, *20*, 16880−16891.

(24) Kayes, B. M.; Nie, H.; Twist, R.; Spruytte, S. G.; Reinhardt, F.; Kizilyalli, I. C.; Higashi, G. S. 27.6% conversion efficiency, a new record for single-junction solar cells under 1 sun illumination. *Proc. PVSC* **2011**, 4−8.

(25) Steiner, M. A.; Geisz, J. F.; Garcia, I.; Friedman, D. J.; Duda, A.; Kurtz, S. R. Optical enhancement of the open-circuit voltage in high quality GaAs solar cells. *J. Appl. Phys.* **2013**, *113*, 123109.

(26) Catrysse, P. B.; Fan, S. Nanopatterned metallic films for use as transparent conductive electrodes in optoelectronic devices. *Nano Lett.* **2010**, *10*, 2944−2949.

(27) Van de Groep, J.; Spinelli, P.; Polman, A. Transparent conducting silver nanowire networks. *Nano Lett.* **2012**, *12*, 3138−3144.